

# PCCP

Accepted Manuscript



This is an *Accepted Manuscript*, which has been through the Royal Society of Chemistry peer review process and has been accepted for publication.

*Accepted Manuscripts* are published online shortly after acceptance, before technical editing, formatting and proof reading. Using this free service, authors can make their results available to the community, in citable form, before we publish the edited article. We will replace this *Accepted Manuscript* with the edited and formatted *Advance Article* as soon as it is available.

You can find more information about *Accepted Manuscripts* in the [Information for Authors](#).

Please note that technical editing may introduce minor changes to the text and/or graphics, which may alter content. The journal's standard [Terms & Conditions](#) and the [Ethical guidelines](#) still apply. In no event shall the Royal Society of Chemistry be held responsible for any errors or omissions in this *Accepted Manuscript* or any consequences arising from the use of any information it contains.

**The effect of thermal annealing in the charge transfer dynamics of a donor-acceptor copolymer and fullerene: F8T2 and F8T2:PCBM**

Yunier Garcia-Basabe,<sup>a,\*</sup> Natasha A. D. Yamamoto,<sup>b</sup> Lucimara S. Roman<sup>b</sup> and

Maria Luiza M. Rocco<sup>a,\*</sup>

*<sup>a</sup>Institute of Chemistry, Federal University of Rio de Janeiro, Rio de Janeiro, 21941-909, Brazil*

*<sup>b</sup>Department of Physics, Federal University of Paraná, Curitiba, 81531-990, Brazil*

\*Corresponding author. Tel.: +55-21-3938-7786; Fax: +55-21-3938-7265.

E-mail address: yunier@iq.ufrj.br (Y. Garcia-Basabe).

luiza@iq.ufrj.br (M.L.M.Rocco)

**Abstract**

Ultrafast charge delocalization dynamics in internal donor-acceptor copolymer poly(9,9-dioctylfluorenyl-co-bithiophene) (F8T2) and its blend with the fullerene derivative [6,6]-phenyl C<sub>61</sub> butyric acid methyl ester (PCBM) was studied by the resonant Auger spectroscopy measured around sulfur *K*-edge using the core-hole clock approach. The effect of thermal annealing on the charge transfer delocalization times ( $\tau_{CT}$ ) was also investigated. Two main transitions with S 1s  $\rightarrow\pi^*$  and S 1s  $\rightarrow\sigma^*(S-C)$  character were measured at the S 1s NEXAFS spectra. Poor charge delocalization was observed for as cast polymeric films at photon energies corresponding to the S 1s  $\rightarrow\pi^*$  transition, which may suggest a weak  $\pi$ -electronic coupling due to weak polymer crystallinity and chain stacking. Enhancement in the charge transfer process for photon energies close to the resonance maximum was observed for thermal annealed F8T2 and its blends. Atomic Force Microscopy (AFM) topography for as cast F8T2:PCBM shows a top position of PCBM units relative to the polymer, homogeneously distributed in the film surface. This configuration improves the charge delocalization through S 1s  $\rightarrow\pi^*$  molecular orbital for the as cast blended film, suggesting a strong  $\pi$ -electronic coupling. A new rearrangement of F8T2:PCBM film was found after thermal annealing, leading to a more efficient electron transfer channel through  $\sigma^*$  molecular orbitals.

## 1. Introduction

Conjugated semiconductor polymers have been subject of several studies for organic photovoltaic applications, such as organic light-emitting diodes and organic solar cells.<sup>1-3</sup> In the last decade internal donor-acceptor copolymers emerged as the most promising polymers for organic solar cell applications. Photovoltaic devices with power conversion efficiency (PCE) higher than 10% have been achieved using these polymers as active layer.<sup>4-9</sup> An important aspect that has been poorly studied for these copolymers is the electron charge transfer (CT) dynamics of excited states occurring in the time scale of femtoseconds ( $10^{-15}$  s). Such studies are important for the understanding of exciton dissociation and electron transport in these materials.

The study of ultrafast charge transfer dynamics can be performed using two different methods: the pulse laser pump-probe<sup>10,11</sup> technique or by the so-called core-hole clock (CHC) approach.<sup>12,13</sup> In the first method, a laser pulse is used for the creation of the excited state, while a second pulse with a delay time is employed for investigating the excited state. The time resolution of this method is limited by the extension of the pump and probe laser pulses and delay time between them. The second method is a synchrotron-based approach, in which the core-hole lifetime of core levels is used as an internal clock. This is an element-sensitive spectroscopy based on the study of core-hole decay spectra, which is a spectral signature characteristic of the system. Different behavior can be observed in the decay spectra when the excited electron is localized in the atom and when it is transferred out of the atom during core-hole lifetime. In the first case, two different final states can be reached: the spectator ( $2h1e$ ) state, where the excited electron does not participate in the decay process, and the participator ( $1h$ ) state, where the excited electron is involved in the core-hole decay, both autoionizing processes known as resonant contributions. The second case corresponds to a two holes ( $2h$ ) final state, called normal Auger or non-resonant Auger

contribution, similar to the decay following ionization. Resonant and non-resonant contributions can be identified in the decay spectra if the so-called Auger resonant Raman condition<sup>14, 15</sup> (exciting photon bandwidth is narrow compared to the natural-lifetime broadening of the core-excited state) is achieved. In this case, kinetic energy dispersion is observed for the resonant contribution, while for the non-resonant contribution it remains unchanged when the incoming photon energy is tuned across an atomic absorption edge.

The charge transfer time ( $\tau_{CT}$ ) represents a quantitative information about the electronic coupling of the system under investigation. It is calculated from the branching ratio of the resonant and non-resonant Auger decay channels and using the natural lifetime ( $\tau_{CH}$ ) of the core-excited state as an internal reference clock:  $\tau_{CT}=(I_{resonant}/I_{non-resonant})*\tau_{CH}$ .<sup>12</sup> A schematic representation of the core-hole clock method is shown in Scheme 1.

### Scheme 1

Recent publications<sup>16-19</sup> applying the CHC method for thiophene-based polymers studied the effect of molecular orientation, thermal annealing and morphology in the charge transfer dynamics. In the present work we extended this approach to the study of poly(9,9-dioctylfluorenyl-co-bithiophene) (F8T2) and its blend with the fullerene derivate [6,6]-phenyl C<sub>61</sub> butyric acid methyl ester (PCBM). The F8T2 is a fluorene-based block copolymer containing the electron-rich bithiophene unit (see Scheme 2). The absorption in the blue region of F8T2 makes it an excellent donor polymer to mix with an acceptor (i.e. fullerene derivatives) forming a system with a broad absorption. Several reports show good photovoltaic device characteristics using this polymer as active layer, especially after thermal annealing.<sup>20-24</sup> Therefore, the effect of thermal annealing in the charge transfer dynamic is an important topic and will be investigated here for thin films of this polymer and its blends. For that we applied the Resonant Auger Spectroscopy (RAS) around sulfur

*K*-absorption edge. *S*-1s NEXAFS spectra were also measured to investigate the unoccupied electronic density of states and to select the excitation energies for collecting the RAS spectra.

## Scheme 2

## 2. Experimental Section

Film preparation was described previously by Macedo *et al.*<sup>24</sup>. The F8T2 film was prepared by dissolving it in chlorobenzene and spin-coating it at 900 rpm for 60 s under nitrogen atmosphere, onto pre-cleaned patterned indium tin oxide coated glass substrates (ITO/Glass). Similar procedure was employed for the F8T2:PCBM (1:3) blend; in this case the chlorobenzene solution containing the blend was stirred for 2 h at 50°C in a sealed flask. Film thickness of 71 nm and 110 nm were measured using Dektak 150 profilometer (Veeco Instruments) for F8T2 and F8T2:PCBM samples, respectively. The thermal treatment at 200°C was performed in vacuum by 20 minutes, after deposition. F8T2-S20 and F8T2:PCBM-S20 labels will be used to refer to as cast polymer and its blend, respectively. The thermal annealed films will be identified as F8T2-S200 and F8T2:PCBM-S200.

Near edge X-ray absorption fine structure (NEXAFS) and resonant Auger decay spectra were measured at the soft X-ray spectroscopy (SXS) beamline at the Brazilian Synchrotron Light Source (LNLS). Si(111) double-crystal monochromator was used to measure TEY NEXAFS (drain current at the sample) and decay spectra covering sulfur 1s-edge. The beamline details have been reported elsewhere.<sup>17, 18</sup> An experimental condition with a photon bandwidth of 0.38 eV was chosen here to reach the Auger Raman condition at the S-K shell (0.59 eV). NEXAFS final data were normalized by a photon flux current (Au

grid) to correct for fluctuations in beam intensity. The energy calibration was performed by taking the well-known value for the  $L_{III}$  transition ( $2p_{3/2} \rightarrow 4d$ ) of metallic molybdenum.

Resonant Auger spectra (RAS) were measured at the same ultrahigh vacuum chamber (UHV) with a base pressure of  $10^{-8}$  mbar equipped with a hemispherical electron energy analyzer. The take-off direction of Auger electrons was  $45^\circ$  and the pass energy 20 eV. The binding energy scale was calibrated using Au ( $4f_{7/2}$ ) signal. A linear combination of Gaussian (G) and Lorentzian (L) profile shape functions was used in the fitting of the spectra, following the same procedure reported before.<sup>17,18</sup> The background correction was performed using a Shirley function. No radiation damage was observed on the time scale of the photoabsorption and photoemission measurements.

### 3. Results and Discussion

S 1s NEXAFS spectra for F8T2-S20, F8T2-S200, F8T2:PCBM-S20 and F8T2:PCBM-S200 samples are shown in Figures 1(a-d), respectively. The features observed in these spectra are very similar to those reported previously by Garcia-Basabe *et al.*<sup>17</sup> for electrochemically deposited polythiophene and polybithiophene polymers. The shoulder at 2471.8 eV and the sharp intense peak at 2472.6 eV are assigned to S 1s  $\rightarrow \pi^*$  and S 1s  $\rightarrow \sigma^*(S-C)$  transitions, respectively, of the thiophene unit. The broad band at higher photon energy is assigned to  $\sigma^*$  shape resonance excitation.

#### Figure 1

In order to extract dynamic information from our spectroscopic data with regard to charge transfer times and also to evaluate the effect of the annealing process sulphur  $KL_{2,3}L_{2,3}$  Auger decay spectra were recorded at different photon energies around S-1s resonance. Figures 2 and 3 show S  $KL_{2,3}L_{2,3}$  resonance Auger spectra (RAS) measured at

eight photon energies (labeled 1-8 in Figure 1) for as-cast F8T2-S20 (a), and annealed F8T2-S200 (b) polymers. The RAS spectrum measured at 2482 eV photon energy (labeled 9 in Figure 1) was used to identify the non-resonant contribution; it is presented in Figure SI1 in Supporting Information File. Four features are contributing to the S  $KL_{2,3}L_{2,3}$  RAS spectra. The assignment of these signals was performed considering previous reported data on thiophene-based polymers.<sup>16,17</sup> The features appearing at kinetic energies of 2107 and 2112 eV are attributed to  $^1S_0$  and  $^1D_2$  normal Auger components. The  $^1S_0$  component is not considered in the quantitative analysis. The other two features are attributed to spectator electrons arising from the  $1s-\pi^*$  and  $1s-\sigma^*$  transitions and named SP1 and SP2, respectively. A new signal appearing at 2116.5 eV kinetic energy was observed in the RAS spectrum measured at 2474.1 eV excitation energy, which is close to the S-1s IP (2475.5 eV). This contribution is assigned to Rydberg states appearing close to the continuum. The increase of the kinetic energy with photon energy excitation was observed for SP1 and SP2 spectator contributions (see Figure SI2 in Supporting Information). FWHM vs photon energy was also presented in Figure SI2, showing a clear line sharpening of the SP1 and SP2 spectator peaks for the photon energies corresponding to  $1s-\pi^*$  and  $1s-\sigma^*$  transitions. The kinetic energy shift and width sharpening are consequences of the Auger resonant Raman condition of resonant (spectator) Auger peaks.<sup>25,26</sup> The peak fitting was performed using the same procedure reported before.<sup>17-19</sup> Here, as reported previously for molecules and polymers containing third-row elements<sup>17-19, 25,27</sup>, the S  $KL_{2,3}L_{2,3}$  participator contribution has very small cross-section and hence only spectator channels are considered in the assignment of the RAS spectra. The overall evolution of these features by increasing the incident photon energy is shown in Figure 4. The intensity of the normal Auger signal increases, reaching ~ 50% for excitation energies (2474.1 eV) close to Rydberg states. The area of both spectator

contributions (SP1 and SP2) reproduces the profile of the NEXAFS spectra, achieving its maximum at photon energies close to  $1s-\pi^*$  (SP1) and  $1s-\sigma^*$  (SP2) transitions.

**Figure 2**

**Figure 3**

**Figure 4**

Charge transfer times ( $\tau_{CT}$ ) for the F8T2 polymer without and with thermal annealing at 200 °C were evaluated using the ratio between the intensities of the resonant spectator (SP1 and SP2) and non-resonant normal Auger (CT) signals using the rate equation  $\tau_{CT}=(I_{\text{spectator}}/I_{\text{normal}})*\tau_{CH}$ , where  $\tau_{CH} = 1.27$  fs represents S 1s core-hole lifetime.<sup>28</sup> The  $\tau_{CT}$  values calculated for photon energies marked as 1-8 in Figure 1 for F8T2 and F8T2-S200 polymers are presented in Table 1. For those RAS spectra collected at photon energies below the resonance maximum at 2472.6 eV, the non-resonant contribution is lower than 10% of the total signal, which limits the accuracy of the  $\tau_{CT}$  determination.<sup>12</sup> A slight improvement in the charge transfer process is observed with the thermal treatment at 200 °C for photon energies close to the resonance maximum, which can be attributed to an increase in film ordering as seen before in similar studies for other internal donor-acceptor copolymers.<sup>19</sup> The  $\tau_{CT}$  values obtained at resonance maximum ( $1s-\sigma^*$ ) are in the same order of those found for other thiophene-based polymers.<sup>16-18</sup> Moreover, it is known that F8T2 chains crystallize after annealing at high temperatures ( $T > 120^\circ\text{C}$ )<sup>20, 21</sup> facilitating the charge transport across the polymer chains. The study of the thermal annealing effect in the morphology of the F8T2 film spin coated using 1,2,4-trichlorobenzene (TCB) solvent shows that it forms a lamella-like crystallites with stacking conformation at high

temperatures.<sup>20,21,23,29</sup> However, high values of the  $\tau_{CT}$  ( $\tau_{CT} > 10\tau_{CH}$ ) for  $1s-\pi^*$  excitation energy have been also found for the thermal annealed F8T2-S200 film. We suggest that this behavior is associated with the fact that the polymer chain stacking in this film is not enough to promote an efficient interchain  $\pi-\pi^*$  charge transfer. The film stacking degree is also dependent on kinetic parameters. Then, the thermal annealing conditions we employed (200°C, 20 minutes in vacuum) may be not sufficient to enable strong polymer chain stacking as it is indicated by the films morphology displayed in Figure 5 (a) and (b) for F8T2 and F8T2-S200 samples, respectively.

### Table 1

### Figure 5

$S-KL_{2,3}L_{2,3}$  RAS spectra measured for photon energies around S-1s absorption edge for the blends are presented in Figures SI3 and SI4. Two spectators and one normal Auger features were also observed. Following the same procedure for the as cast (F8T2:PCBM-S20) and thermal annealed (F8T2:PCBM-S200) blended films, the peak area plot against the photon energy and  $\tau_{CT}$  values obtained from the RAS spectra are reported in Figure 6 and Table 2, respectively. Peak areas of both spectator contributions (SP1 and SP2) reproduce as well the profile of the NEXAFS spectrum, as previously discussed in Figure 4. For the F8T2:PCBM-S20 film, the charge transfer dynamics at  $1s-\pi^*$  excitation energy is better than  $1s-\sigma^*$ . Similar behavior was found for poly[2,7-(9,9-bis(2-ethylhexyl)-dibenzosilole)-alt-4,7-bis(thiophen-2-yl)benzo-2,1,3-thiadiazole] blended with PCBM.<sup>18</sup> This may be associated with the fact that for this film the PCBM are positioned above the polymer chains, favoring the charge transfer through  $\pi^*$  orbitals. This is corroborated by the results presented in Figure 7, which shows AFM images of as cast and annealed F8T2:PCBM films. The as cast samples present spherical domains homogeneously distributed in the film while

in the annealed samples a chain-like structure starts to be formed. Previous report on photoluminescence studies also point out for improvement in the charge transfer process for blended F8T2 polymer with PCBM without any thermal annealing treatment.<sup>20,21,23,29</sup> Significant improvement in the charge transfer dynamics was achieved by the annealed F8T2:PCBM-S200 film at excitation energies close to  $1s-\sigma^*$  (4 and 5 photon energies in Figure 1) where the charge transfer process enhanced in  $\sim 40\%$ . On the other hand, only a small difference is observed for  $1s-\pi^*$  resonance between thermal and non-thermal annealed blends. It is known that thermal annealing at high temperatures cause film rearrangement.<sup>11,20,30</sup> In many cases, higher temperature treatments favor PCBM cluster formation. For example, Huang *et al.*<sup>20,21</sup> reported that after thermal annealing at  $250^\circ\text{C}$  clusters of PCBM units are surrounded by F8T2 layers, while for as cast blends the PCBM domains are homogeneously distributed in the film. Therefore, the improvement in charge transfer dynamics obtained for excitation energies close to  $1s-\sigma^*$  after thermal annealing may be attributed to a new configuration in the blend, which enhances the electron delocalization through this orbital. Borges Jr. *et al.*<sup>31</sup> performed theoretical investigations on the charge transfer states for a low band gap system poly(thieno[3,4-b]-thiophene benzodithiophene) (PTB1) blended with C60. They found better charge delocalization for a configuration containing two stacked PBT1 trimer chains with C60 in lateral position.

**Figure 6**

**Figure 7**

**Table 2**

The  $\tau_{\text{CT}}$  reported in Tables 1 and 2 decreases with the increase of the photon energy after resonance maximum. The  $\tau_{\text{CT}}$  magnitude depends on several factors as: the shape of the tunneling barrier, the energetic position of the resonance level, and the density of

unoccupied states in the vicinity into which the electron can tunnel.<sup>32</sup> The shape of the tunneling barrier plays a more important role at higher energies. So, the similar  $\tau_{CT}$  values observed for the four polymeric films may be correlated with a similar shape of the tunneling barrier in these films.

#### 4. Conclusions

The core-hole-clock approach in the framework of the resonant Auger spectroscopy was employed to investigate the ultrafast charge transfer dynamics for the internal donor-acceptor poly(9,9-dioctylfluorenyl-co-bithiophene) (F8T2). The effect of thermal annealing and the formation of blends with PCBM were monitored through the charge transfer times ( $\tau_{CT}$ ). Unoccupied electronic density of states evaluated by S-1s NEXFS spectra show two main transitions:  $S\ 1s \rightarrow \pi^*$  and  $S\ 1s \rightarrow \sigma^*(S-C)$ . The  $\tau_{CT}$  were calculated detuning the photon energy around S-1s absorption edge. Poor charge delocalization was observed for the polymeric films (F8T2-S20 and F8T2-S200) at photon energies involving  $1s \rightarrow \pi^*$  transition, suggesting weak  $\pi$ - $\pi$  stacking limiting this electron transfer channel. Enhancement in the charge transfer process was observed after thermal annealing for the polymer and its blend for photon energies close to resonance maximum. The as cast blend produced with the electron acceptor PCBM unit improves the charge delocalization through  $S\ 1s \rightarrow \pi^*$  molecular orbital. This suggests a good interface between PCBM and F8T2 phases with PCBM nanospheres in a vertical position relative to the polymer, as was observed by AFM images. A new rearrangement with a chain-like structure after thermal annealing with PCBM improves the charge delocalization through  $\sigma^*$  molecular orbitals. Due to the fact that the  $\tau_{CT}$  values obtained at higher excitation energies are similar for the four samples, we suggest that thermal annealing and the blending of the F8T2 polymer with PCBM did not affect the shape of the electron tunneling barrier.

## 5. Acknowledgments

Research partially supported by LNLS – National Synchrotron Light Laboratory, Brazil.

M.L.M.R. and L.S.R. would like to thank CNPq for financial support. The authors would also like to acknowledge CNPq, CAPES, and the technical assistance of the soft X-ray group from LNLS. Y.G.-B. would like to thank CNPq for a PDJ scholarship.

## References

1. H. Klauk, *Chem. Soc. Rev.*, 2010, **39**, 2643-2666.
2. Y.-J. Cheng, S.-H. Yang and C.-S. Hsu, *Chem. Rev.*, 2009, **109**, 5868-5923.
3. G. Li, R. Zhu and Y. Yang, *Nature Photon.*, 2012, **6**, 153-161.
4. S. H. Park, A. Roy, S. Beaupre, S. Cho, N. Coates, J. S. Moon, D. Moses, M. Leclerc, K. Lee and A. J. Heeger, *Nature. Photon.*, 2009, **3**, 297-302.
5. Sun. Y, C. J. Takacs, S. R. Cowan, J. H. Seo, X. Gong, A. Roy and A. J. Heeger, *Adv. Mater.*, 2011, **23**, 2226-2230.
6. Y. Sun, G. C. Welch, W. L. Leong, C. J. Takacs, G. C. Bazan and A. J. Heeger, *Nature Mater.*, 2012, **11**, 44-48.
7. M. A. Green, K. Emery, Y. Hishikawa, W. Warta and E. D. Dunlop, *Prog. Photovoltaics*, 2011, **19**, 565-572.
8. D. C. Borrelli, M. C. Barr, V. Bulovic and K. K. Gleason, *Sol. Energy Mater. Sol. Cells*, 2012, **99**, 190-196.
9. J. You, L. Dou, K. Yoshimura, T. Kato, K. Ohya, T. Moriarty, K. Emery, C.-C. Chen, J. Gao, G. Li and Y. Yang, *Nat. Commun.*, 2013, **4**, 1-10.
10. R. Weinkauff, L. Lehr, E. W. Schlag, S. Salzmann and C. M. Marian, *Phys. Chem. Chem. Phys.*, 2008, **10**, 393-404.
11. R. A. Marsh, J. M. Hodgkiss, S. Albert-Seifried and F. R. H., *Nano Lett.*, 2010, **10**, 923-930.
12. D. Menzel, *Chem. Soc. Rev.*, 2008, **37**, 2212-2223.
13. R. Friedlein, S. Braun, M. P. de Jong, W. Osikowicz, M. Fahlman and W. R. Salaneck, *J. electron spectrosc*, 2011, **183**, 101-106.
14. F. Gel'mukhanov and H. Agren, *Phys. Rev. A.*, 1996, **54**, 3960-3970.
15. M. N. Piancastelli, *J. Electron Spectrosc. Relat. Phenom.*, 2000, **107**, 1-26.
16. C. Arantes, B. Beck, B. G. A. L. Borges, G. Araújo, L. S. Roman and M. L. M. Rocco, *J. Phys. Chem. C*, 2013, **117**, 8208-8213.
17. Y. Garcia-Basabe, B. G. A. L. Borges, D. C. Silva, L. Micaroni, L. S. Roman and M. L. M. Rocco, *Org. Electron.*, 2013, **14**, 2980-2986.
18. Y. Garcia-Basabe, C. F. N. Marchiori, B. G. A. L. Borges, N. A. D. Yamamoto, A. G. Macedo, M. Koehler, L. S. Roman and M. L. M. Rocco, *J. Appl. Phys.*, 2014, **115**, 134901.

19. Y. Garcia-Basabe, C. F. N. Marchiori, C. E. de Moura, A. B. Rocha, L. S. Roman and M. L. M. Rocco, *J. Phys. Chem. C*, 2014, **118**, 23863–23873.
20. J.-H. Huang, C.-Y. Yang, Z.-Y. Ho, D. Kekuda, M.-C. Wu, F.-C. Chien, P. Chen, C.-W. Chu and K.-C. Ho, *Org. Electron.*, 2009, **10**, 27-33.
21. J.-H. Huang, Z.-Y. Ho, D. Kekuda, Y. Chang, C.-W. Chu and K.-C. Ho, *Nanotechnology* 2009, **20**, 1-9.
22. D. Kekuda, J.-H. Huang, K.-C. Ho and C.-W. Chu, *J. Phys. Chem. C*, 2010, **114**, 2764–2768.
23. J.-H. Huang, C.-P. Lee, Z.-Y. Ho, D. Kekuda, C.-W. Chu and K.-C. Ho, *Sol. Energy Mater. Sol. Cells*, 2010, **94**, 22–28.
24. A. G. Macedo, D. C. Silva, N. A. D. Yamamoto, L. Micaroni, R. M. Q. Mello and L. S. Roman, *Synth. Met.*, 2013, **170**, 63–68.
25. K. Yoshii, Y. Baba and T. A. Sasaki, *Phys. Stat. Sol.*, 1998, **206**, 811-822.
26. M. N. Piancastelli, G. Goldsztejn, T. Marchenko, R. Guillemin, R. K. Kushawaha, L. Journal, S. Carniato, J.-P. Rueff, D. Céolin and M. Simon, *J. Phys. B: At. Mol. Opt. Phys.*, 2014, **47**, 1-6.
27. Y. Baba, T. A. Sasaki and H. Yamamoto, *Phys. Rev. B*, 1994, **49**, 709-711.
28. J. L. Campbell and T. Papp, *Atomic Data and Nuclear Data Tables* 2001, **77**, 1-56
29. F. Huang, K.-S. Chen, H.-L. Yip, S. K. Hau, O. Acton, Y. Zhang, J. Luo and A. K.-Y. Jen, *J. Am. Chem. Soc.*, 2009, **131**, 13886–13887.
30. E. Verploegen, R. Mondal, C. J. Bettinger, S. Sok, M. F. Toney and Z. Bao, *Adv. Funct. Mater.*, 2010, **20**, 3519–3529.
31. I. Borges Jr, A. J. A. Aquino, A. Köhn, R. Neiman, W. L. Hase, L. X. Chen and H. Lischka, *J. Am. Chem. Soc.*, 2013, **135**, 18252–18255.
32. W. Wurth and D. Menzel, *Chem. Phys.*, 2000, **251**, 141–149.

## Tables

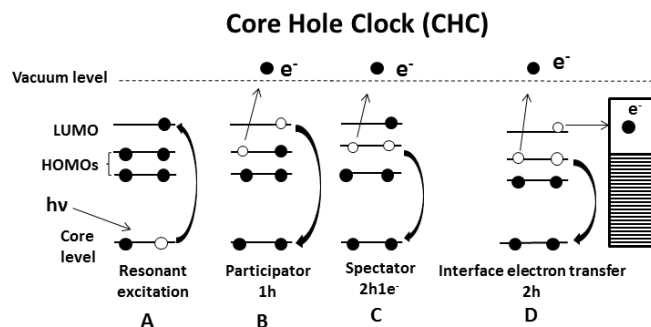
**Table 1.** Charge transfer times ( $\tau_{CT}$ ) values for photon energies labeled 1-8 in the NEXAFS spectra for F8T2-S20 and F8T2-S200 polymers.  $\tau_{CT}$  standard deviation values are shown in parentheses.

Label	Photon energy (eV)	$\tau_{CT}$ (fs)	
		F8T2-S20	F8T2-S200
1	2471.4	-	-
2 ( <b>1s-<math>\pi^*</math></b> )	2471.8	-	-
3	2472.3	12.6 (4)	10.8 (4)
4 ( <b>1s-<math>\sigma^*</math></b> )	2472.6	10.5 (6)	9.2(6)
5	2472.9	8.0 (5)	7.7(3)
6	2473.1	4.0 (2)	3.8(2)
7	2473.4	3.3(2)	2.5 (3)
8	2474.1	1.1(3)	1.0 (3)

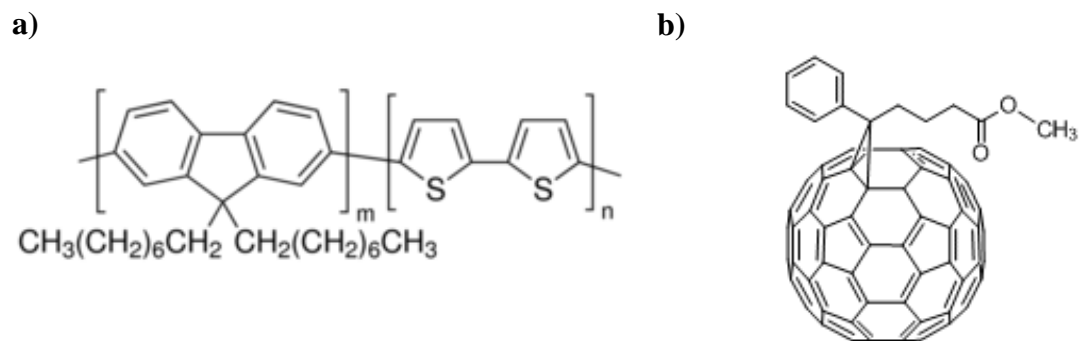
**Table 2.** Charge transfer times ( $\tau_{CT}$ ) values for photon energies labeled 1-8 in the NEXAFS spectra for F8T2:PCBM-S20 and F8T2:PCBM-S200 polymers.  $\tau_{CT}$  standard deviation values are shown in parentheses.

Label	Photon energy (eV)	$\tau_{CT}$ (fs)	
		F8T2:PCBM-S20	F8T2:PCBM-S200
1	2471.4	9.7 (5)	9.6 (4)
2 ( <b>1s-<math>\pi^*</math></b> )	2471.8	8.7 (3)	7.4(4)
3	2472.3	10.3 (4)	9.9 (3)
4 ( <b>1s-<math>\sigma^*</math></b> )	2472.6	9.8 (3)	6.1 (2)
5	2472.9	6.3 (2)	4.1 (3)
6	2473.1	4.0 (3)	3.9 (2)
7	2473.4	2.2 (2)	2.5 (2)
8	2474.1	1.0 (2)	0.9 (3)

## Figures and Schemes



**Scheme 1.** Schematic representation of the core-hole clock method. (A) Core level resonant excitation into an unoccupied molecular orbital, LUMO. (B) Participator decay process  $1h$  final state. (C). Spectator decay process with a  $2h1e$  final state. (D) The electron is transferred to the substrate (or molecular environment) and core-hole decay processes via a normal Auger decay with a  $2h$  final state.



**Scheme 2.** Chemical structure representation of **a)** poly(9,9-dioctylfluorenyl-co-bithiophene) (F8T2) monomer and **b)** fullerene derivate [6,6]-Phenyl C<sub>61</sub> butyric acid methyl ester (PCBM).

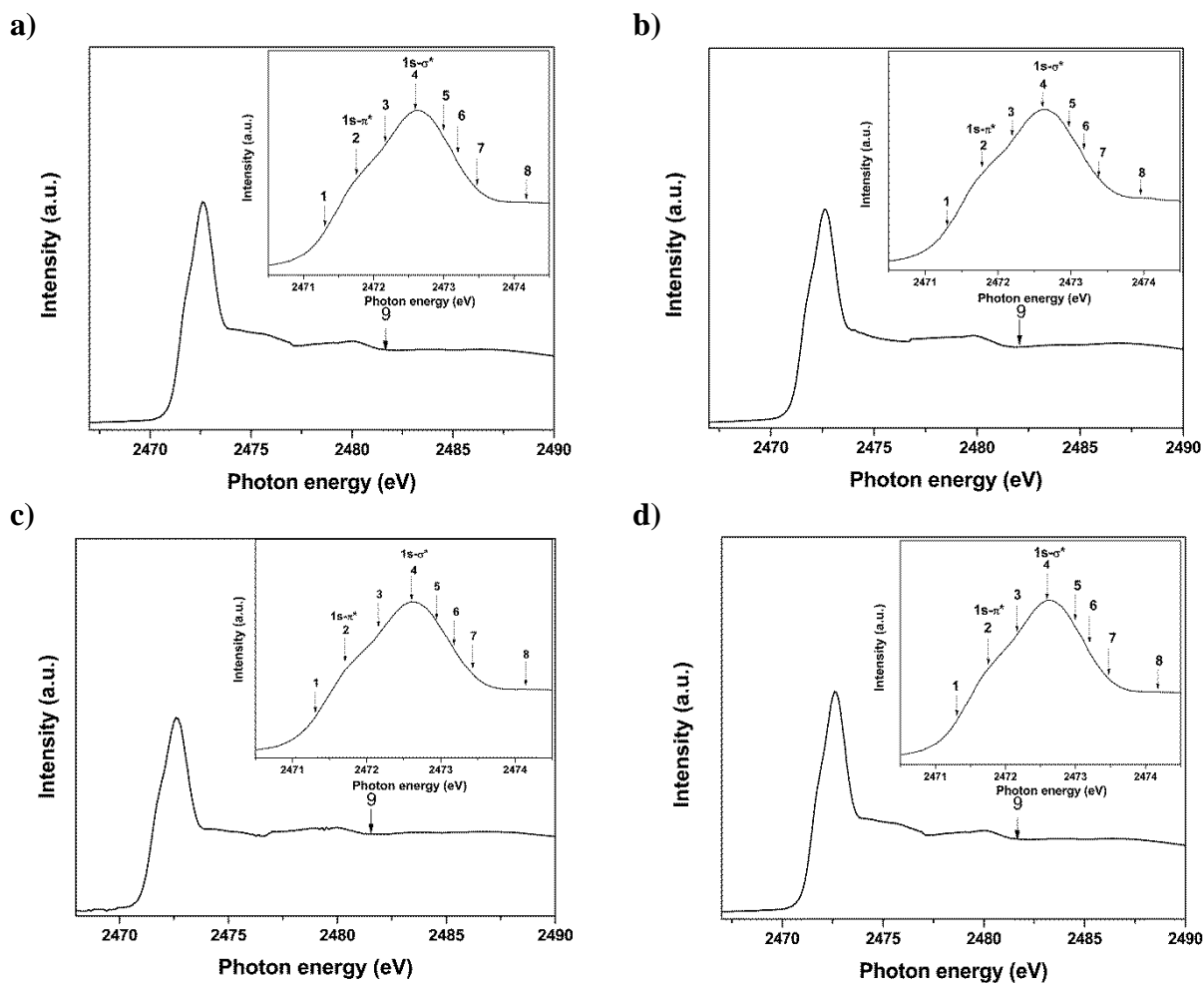


**Figure 1.** Sulphur *K*-edge NEXAFS spectra of F8T2-S20 (a), F8T2-S200 (b), F8T2:PCBM-S20 (c), and F8T2:PCBM-S200 (d). Inset: main transitions region ( $S 1s-\pi^*$  and  $S 1s-\sigma^*$ ).

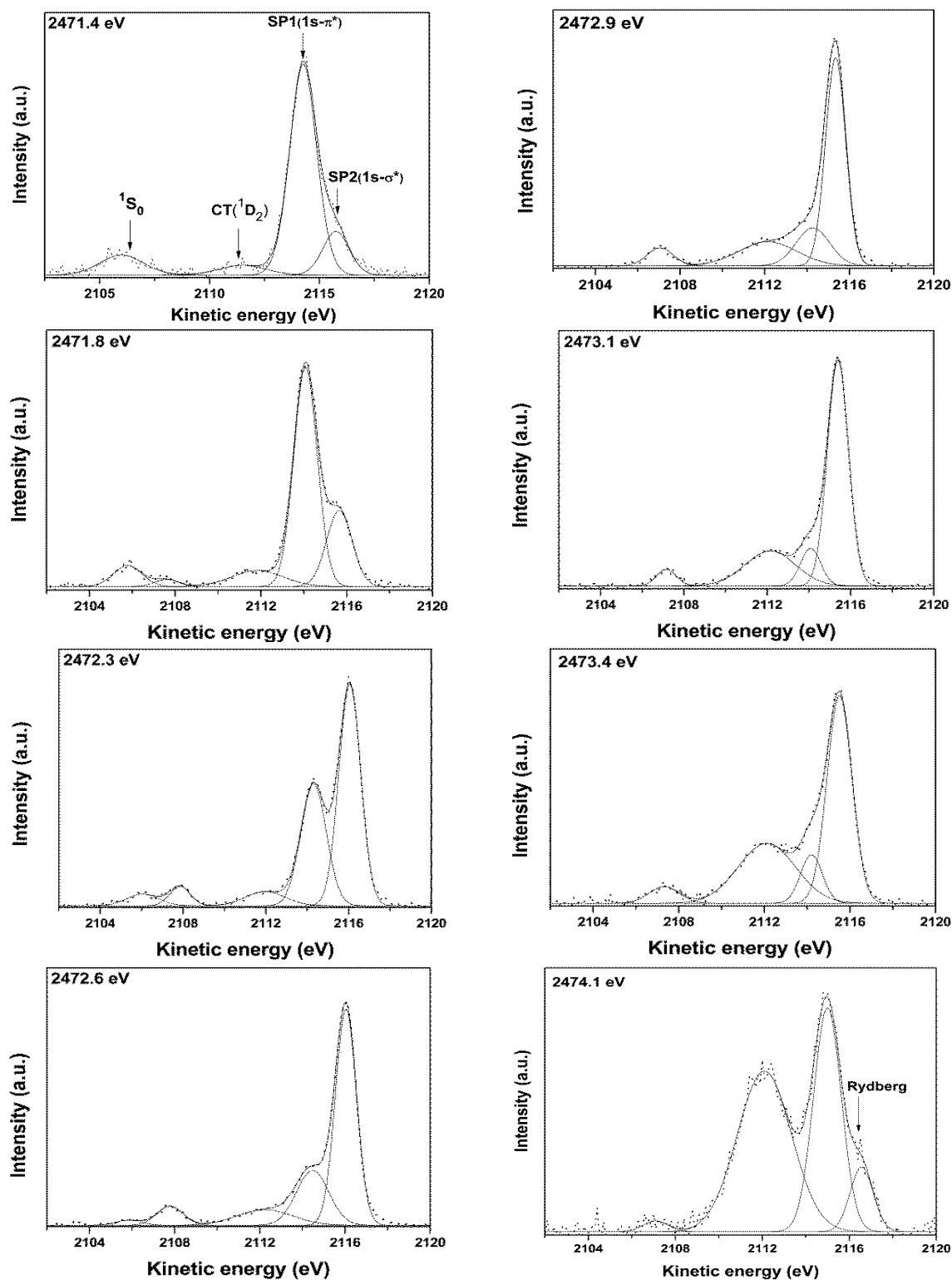


**Figure 2.** Peak fitting procedure of S  $KL_{2,3}L_{2,3}$  RAS spectra measured at different photon energies around S-1s resonance for as-cast F8T2-S20 polymer.

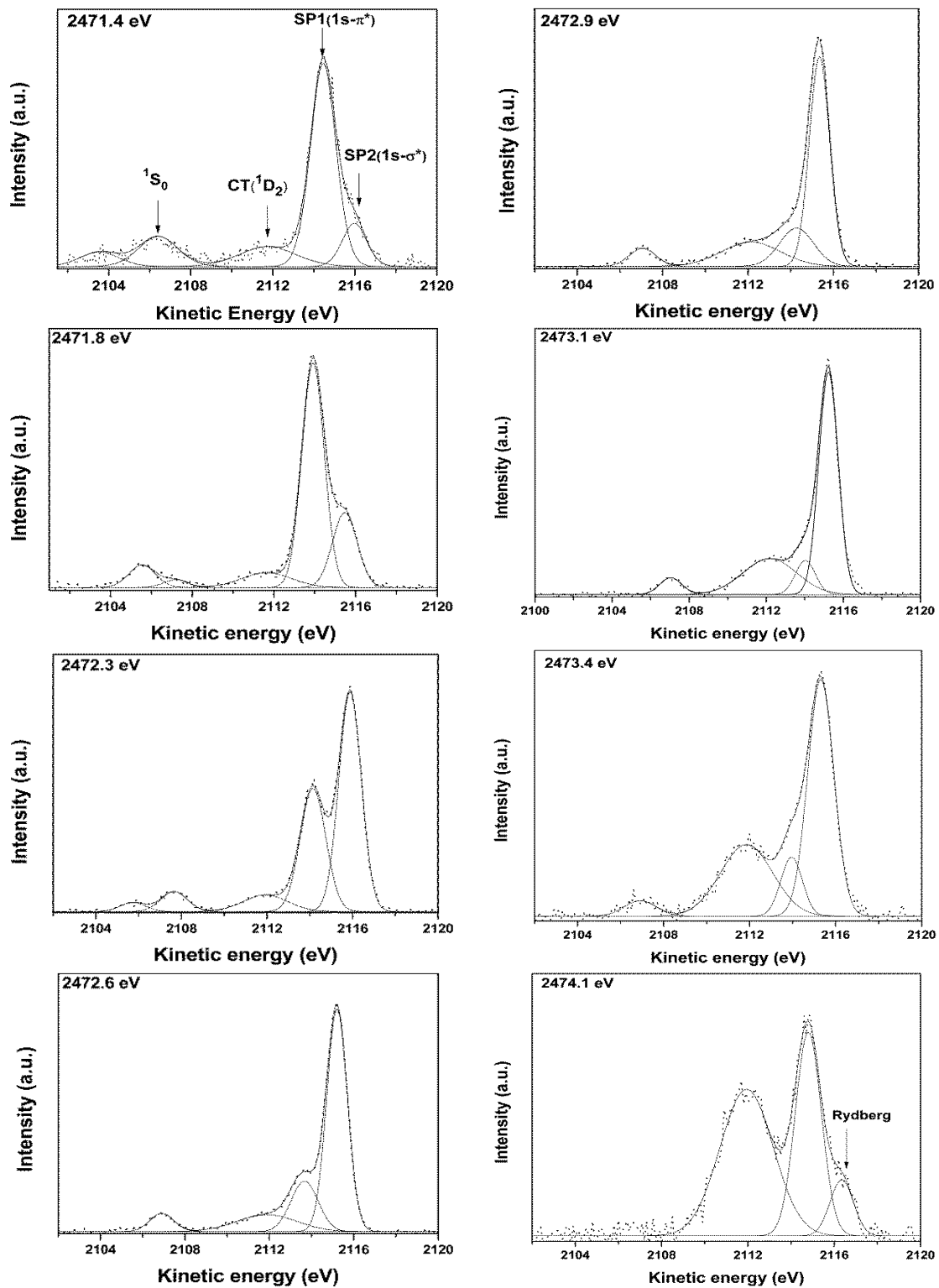


**Figure 3.** Peak fitting procedure of S  $KL_{2,3}L_{2,3}$  RAS spectra measured at different photon energies around S-1s resonance for thermal annealed F8T2-S200 polymer.

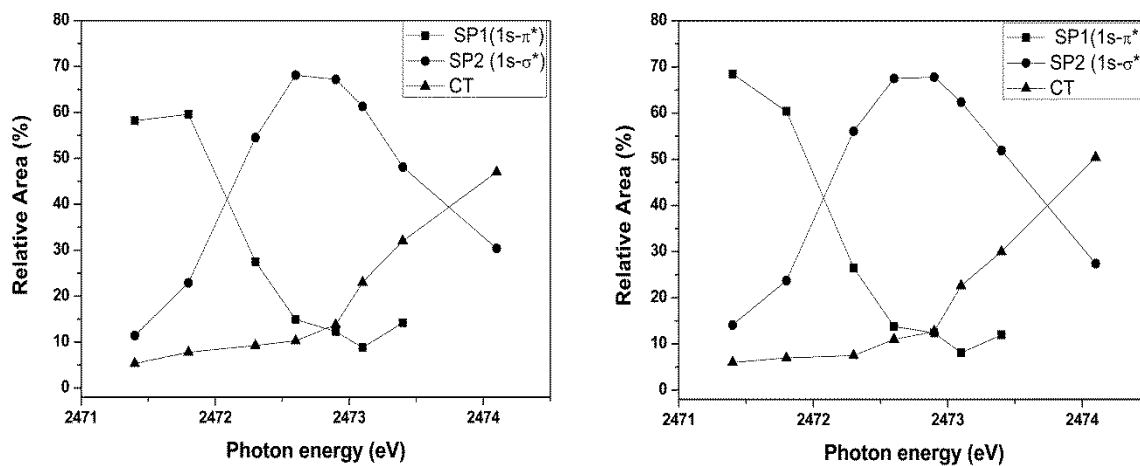


**Figure 4.** Peak area plotted against incident photon energy obtained by deconvolution of the  $S-KL_{2,3}L_{2,3}$  RAS spectra for F8T2-S20 (a), and F8T2-S200 (b) films.

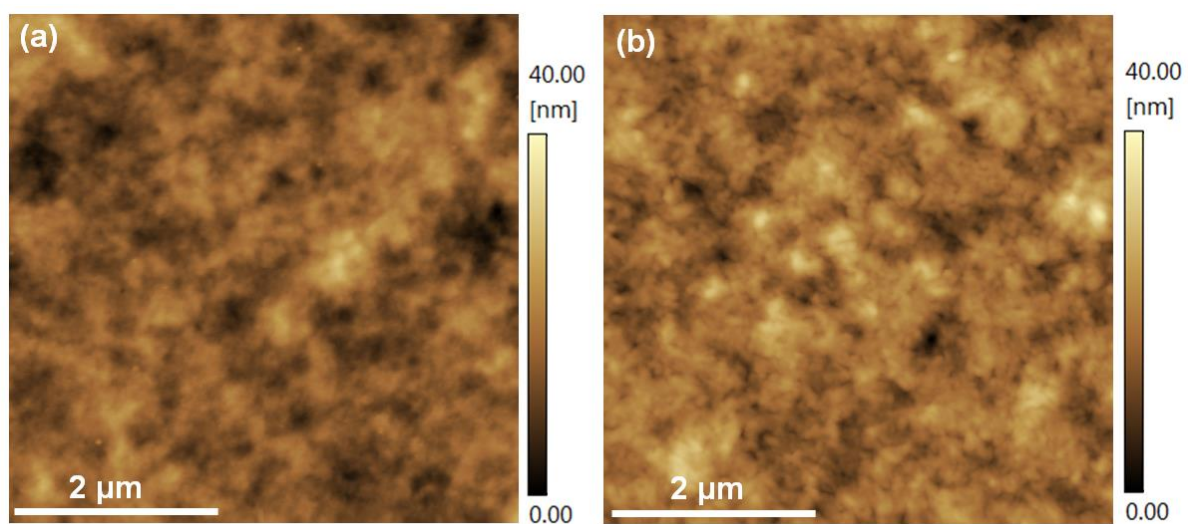


**Figure 5.** Atomic Force Microscopy (AFM) topography of (a) F8T2-S20 and (b) F8T2-S200 coated onto ITO/PEDOT:PSS substrates. The scan size is 5 μm x 5 μm.

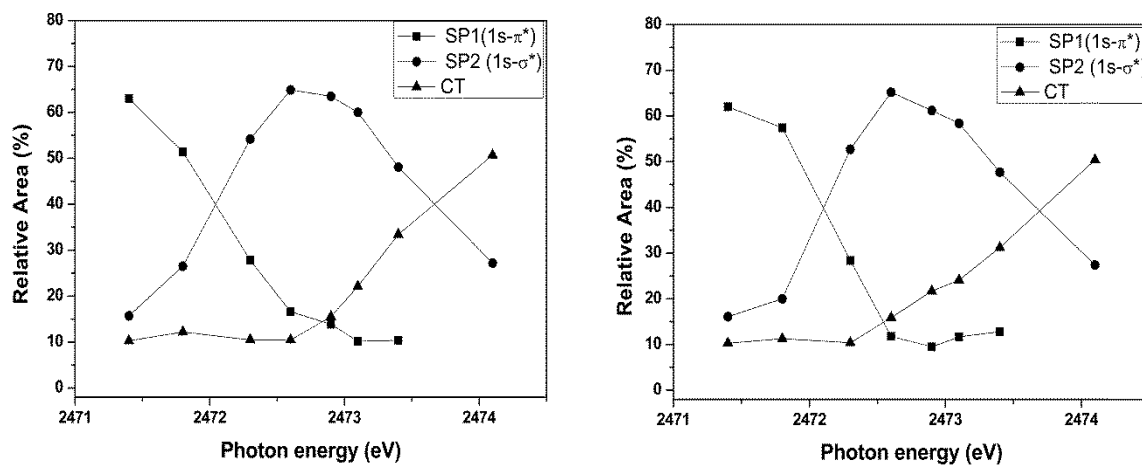


**Figure 6.** Peak area plotted against incident photon energy obtained by deconvolution of the S- $KL_{2,3}L_{2,3}$  decay spectra for F8T2:PCBM-S20 (a), and F8T2:PCBM-S200 (b) films.

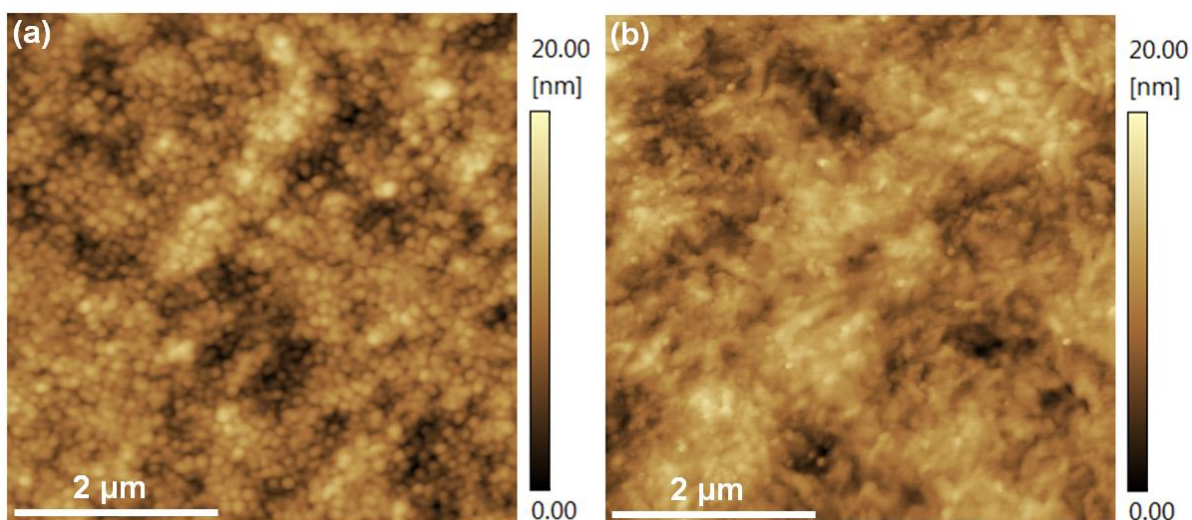


**Figure 7.** Atomic Force Microscopy (AFM) topography of (a) F8T2:PCBM-S20 and (b) F8T2:PCBM-S200 coated onto ITO/PEDOT:PSS substrates. The scan size is 5 μm x 5 μm.